Electronic Structure and Properties of Trihalogen Cations X_3^+ and XY_2^+ (X, Y = F, Cl, Br, I)

Jun Li,[†] Stephan Irle,[‡] and W. H. Eugen Schwarz*

Theoretical Chemistry Laboratory, Department of Chemistry, University of Siegen, D-57068 Siegen, Germany

Received March 14, 1995[⊗]

Electronic structures, charge distributions, geometries, valence force constants, and vibrational frequencies of the homoatomic clusters F_3^+, Cl_3^+, Br_3^+, and I_3^+ and of the heteroatomic clusters ClF_2^+, BrF_2^+, IF_2^+, $BrCl_2^+$, ICl_2^+, and IBr_2^+ were determined. The self-consistent field approach extended by MP2-correlation energy or density-functional corrections was applied using various basis sets. It was found that d- and f-type polarization functions play a crucial role as in some other halogen compounds. The MP2 approach yields the most satisfactory results. The effect of the crystalline environment surrounding the Cl_3^+, Br_3^+, and I_3^+ species is successfully simulated by a Madelung potential. Frequencies calculated in the crystal field are in reasonable agreement with the more reliable ones among the experimental results. Coupling force constants were determined. They are not consistent with some empirical rules. Bonding and charge distributions of the formally mixed-valence systems $X^+Y_2^0$ are discussed. X^+ behaves like a divalent chalcogen with high electronegativity. Each of the X^+-Y bonds in XY_2^+ is very similar to the bond in X−Y. We predict the experimentally unknown F_3^+ to be stable in vacuum but not in the solid state. Structures and frequencies of XY_2^+ species, which are as yet unknown, are also predicted.

1. Introduction

During the past 2 decades, a number of unique compounds containing polyhalogen cluster cations were synthesized.[1−10] Among them, $X_3^+AsF_6^-$ (X = Br, I) (see Figure 1), $XF_2^+SbF_6^-$ (X = Cl, Br), and $ICl_2^+SbF_6^-$ were well-characterized by X-ray structural analyses.[11−18] Many polyhalogen cations were also investigated by vibrational spectroscopy.[3,7] One question is which of the possible XY_2^+ cations (X = central atom, Y = terminal atom) may exist as stable species.

The vibrational properties are rather important in identifying these compounds. However, there are discrepancies among different experimental results.[7,11,19] Furthermore, some force constants need further refinement due to the indeterminacy of the classical force field method in evaluating off-diagonal force constants.[11] Accordingly, the second aim of our investigation is the determination of such experimentally ill-defined parameters.

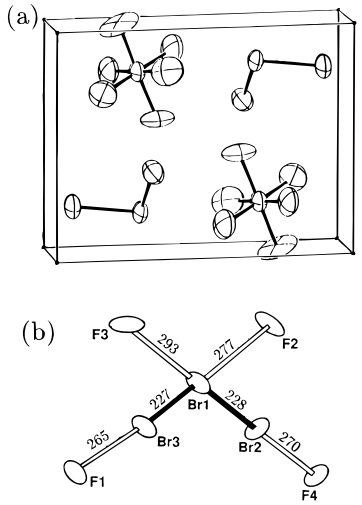

Figure 1. Geometry of Br_3AsF_6:[11] (a) unit cell; (b) Br_3^+ and its four closest F^- neigbors from surrounding AsF_6^-, lying approximately in a plane. Distances in picometer.

Third, the formally mixed-valence character of the homoatomic cluster compounds, $X^+X_2^0$, stimulates the elucidation of the electronic structure and charge distribution of these clusters. Do the valencies and charge distributions vary in the cases of homo- or hetero-halogen cations when going from F to I?

The halogen cluster cations in real compounds are strongly influenced by the electric fields created by the surrounding ions. In addition, the distances between the constituent atoms of the

[†] Permanent address: Fujian Institute of Research on the Structure of Matter, Chinese Academy of Sciences, Fujian, China.

[‡] Present address: Theoretische Chemie, Universität Wien, Währinger Strasse 17, A-1090 Wien, Austria.

[⊗] Abstract published in *Advance ACS Abstracts,* November 1, 1995.

(1) Gillespie, R. J.; Morton, M. J. *Inorg. Chem.* **1970**, *9*, 811; *Inorg. Chem.* **1972**, *11*, 586; *Q. Rev.* **1971**, *25*, 553.
(2) Chung, C.; Cady, G. H. *Inorg. Chem.* **1972**, *11*, 2528.
(3) Gillespie, R. J.; Morton, M. J.; Sowa, J. M. *Adv. Raman Spectrosc.* **1972**, *1*, 539.
(4) Gillespie, R. J.; Kappor, R.; Faggiani, R.; Lock, C. J. L.; Murchie, M.; Passmore, J. *J. Chem. Soc., Chem. Commun.* **1973**, 8.
(5) Davies, C. G.; Gillespie, R. J.; Ireland, P. R.; Sowa, J. M. *Can. J. Chem.* **1974**, *52*, 2048.
(6) Gillespie, R. J.; Passmore, J. *Adv. Inorg. Chem. Radiochem.* **1975**, *17*, 49.
(7) Shamir, J. *Struct. Bonding (Berlin)* **1979**, *37*, 141.
(8) Passmore, J.; Taylor, P.; Whidden, T.; White, P. S. *Can. J. Chem.* **1979**, *57*, 968.
(9) Apblett, A.; Grein, F.; Johnson, J. P.; Passmore, J.; White, P. S. *Inorg. Chem.* **1986**, *25*, 422.
(10) Hartl, H.; Nowicki, J.; Minkwitz, R. *Angew. Chem.* **1991**, *103*, 311.
(11) Christe, K. O.; Bau, R.; Zhao, D. *Z. Anorg. Allg. Chem.* **1991**, *593*, 46.
(12) Passmore, J.; Sutherland, G.; White, P. S. *Inorg. Chem.* **1981**, *20*, 2169.
(13) Gillespie, R. J.; Morton, M. J. *Inorg. Chem.* **1970**, *9*, 616.
(14) Edwards, A. J.; Sills, R. J. C. *J. Chem. Soc. A* **1970**, 2697.
(15) Lynton, H.; Passmore, J. *Can. J. Chem.* **1971**, *49*, 2539.
(16) Christe, K. O.; Schack, C. J. *Inorg. Chem.* **1970**, *9*, 2296.
(17) Edwards, A. J.; Jones, G. R. *J. Chem. Soc. A* **1969**, 1467.
(18) Vonk, C. G.; Wiebenga, E. H. *Acta Crystallogr.* **1959**, *12*, 859.
(19) Chen, L. H.; Nour, E. M.; Laane, J. M. *J. Raman Spectrosc.* **1983**, *14*, 232.

0020-1669/96/1335-0100$12.00/0

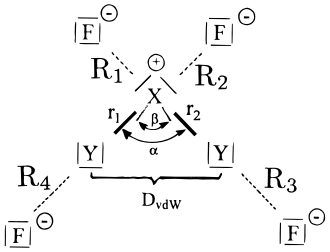

Figure 2. XY_2^+, with sourrounding counterions, schematic: α = linear bonds angle; β = natural hybrids angle.

cluster and the adjacent anions are less than the sums of their van der Waals radii. $Br_3^+AsF_6^-$ [11] is considered as an example. The sums of the van der Waals radii[20] of the atoms Br and F, D_{vdW}, and the "nonbonded" interatomic distances R are D = 320 and R = 265−293 pm; see Figures 1b and 2. For $I_3^+AsF_6^-$ [12] the corresponding values are D = 340 and R = 273−307 pm. The strong interactions increase the difficulties of applying quantum chemical approaches to the cluster cations. The few ab initio calculations in the literature[21−25] have not considered the influence of the surrounding. While the forces between the cluster cation and the surrounding anions (comprising also the attractive dispersion and repulsive Pauli forces as well as orbital interactions of the polarization and charge transfer type, etc.) are of course nonnegligible with respect to thermodynamic stability and lattice energy, we believe that reasonable geometries and force constants can be obtained if the dominant electrostatic interactions are accounted for.

In this paper, in order to elucidate the above mentioned questions, ab initio and density functional calculations have been performed on the free X_3^+ and XY_2^+ (X, Y = F, Cl, Br, and I, with X less electronegative than Y) cluster cations and also on the clusters X_3^+ (X = Cl, Br, and I) embedded in electrostatic crystal fields. Computational details are given in section 2. The free clusters are discussed in section 3. After selection of reliable methods and basis sets, the clusters in the crystal are investigated in section 4. Our conclusions are summarized in section 5.

2. Computational Details

2.1. Methods. Standard ab initio calculations were carried out at the spin-restricted Hartree−Fock (RHF) and correlated MP2 levels[26] using the Gaussian 92/DFT program package.[27] Concerning density functional theories (DFT), we have chosen a pure approach (BLYP) with Becke's exchange functional[28] and the correlation functional of Lee, Yang, and Parr.[29] Since Hartree−Fock-exchange/DFT-exchange-and-correlation hybrids have been found to yield both better geometries and improved SCF convergence behavior for systems with light atoms,[30−34] the so-called Becke 3LYP hybrid procedure "B3LYP"[29,35,36] was also applied, using the default parameter values. A standard grid of about 3000 points per atom was chosen not only for the frequency calculations but also for the geometry optimizations.

Effective core potential (EP), i.e., pseudopotential, valence-only calculations have been performed for all systems in order to keep the computational efforts, especially for the heavier systems, manageable. To assess the reliability, all-electron (AE) calculations were also performed for the lighter systems (F_3^+, Cl_3^+, Br_3^+). The nonrelativistic effective core potentials of Hay and Wadt[37] (NEP) as well as the quasi-relativistic ones of Christiansen et al.[38] or the compact quasi-relativistic ones of Stevens et al.[39] (REP) were applied.

2.2. Basis Sets. Standard basis sets as implemented in the Gaussian 92/DFT program[27] were adopted, such as 3-21, 6-31, and 6-311, as well as the corresponding ones with up to two d and one f polarization functions and one diffuse function. The triple-ζ split-valence basis sets (TZV) of Ahlrichs' group[40] were augmented by one d-type polarization function[41] (TZV(d)). For the NEP calculations, double-ζ (DZ) and double-ζ plus one d function with exponents from the literature[41] were used (DZ(d)), namely, $\alpha_d(F) = 1.496$, $\alpha_d(Cl) = 0.75$, $\alpha_d(Br) = 0.389$, $\alpha_d(I) = 0.266$. For the REP calculations, the triple-ζ 311 (TZ) valence sets of Pacios and Gomez[42] for the F, Cl, and Br atoms and of Stevens et al.[39] for the I atom, with one or two d-type polarization function(s), were used. In each case, + denotes an additional sp-type diffuse function set ($\alpha_{sp}(F) = 0.1076$, $\alpha_{sp}(Cl) = 0.0483$, $\alpha_{sp}(Br) = 0.043$, and $\alpha_{sp}(I) = 0.039$)[43]. In the calculations of the heterohalogen species, TZ+(d) bases were used for the terminal atoms with more electron density and the TZ(d) basis for the central atom with less electron density.

2.3. Analysis. The geometries (r_1, r_2, α) of the free clusters were fully optimized at the respective level of theory, and the force constants and frequencies were then calculated at the same level. In order to express all force constants in the same unit (N/cm), the angle bending coordinates were scaled according to the optimized bond lengths.

In order to estimate the accuracy of the approach, we have also calculated the halogen molecules X_2 at the REP/MP2/TZ+(d) level[44] and compared the results with accurate experimental data.[45] The calculated bond lengths, frequencies, and force constants (see Table 6) are in error by +1.3, ±1.5, and ±3%, respectively. (For fluorine containing species the vibrational parameters are in error by ±5 and ±10%, respectively.)

The bonding situation was analyzed in terms of the traditional Mulliken approach,[46] Weinholds' natural bond orbital (NBO) method,[47] Foster−Boys localized MOs,[48] Bader's method,[49] the present authors'

(20) Porterfield, W. W. *Inorganic Chemistry*; Addison-Wesley: New York, 1984.
(21) Ungemach, S. R.; Schaefer, H. F. *J. Am. Chem. Soc.* **1976**, *98*, 1658.
(22) Bader, R. F. W.; MacDougall, P. J.; Lau, C. D. H. *J. Am. Chem. Soc.* **1984**, *106*, 1594.
(23) Burdett, J. K.; Marsden, C. J. *Nuov. J. Chim.* **1988**, *12*, 797.
(24) Li, Y.; Wang, X.; Jensen, F.; Houk, K. N.; Olah, G. A. *J. Am. Chem. Soc.* **1990**, *112*, 3922.
(25) Lin, Z. Y.; Hall, M. B. *Polyhedron* **1993**, *12*, 1499.
(26) Roothaan, C. C. J. *Rev. Mod. Phys.* **1960**, *32*, 179. Binkley, J. S.; Pople, J. A.; Dobson, P. A. *Mol. Phys.* **1974**, *28*, 1423. Møller, C.; Plesset, M. S. *Phys. Rev.* **1934**, *46*, 618.
(27) Frisch, M. J.; Trucks, G. W.; Schlegel, H. B.; Gill, P. M. W.; Johnson, B. G.; Wong, M. W.; Foresman, J. B.; Robb, M.; Head-Gordon, M.; Replosle, E. S.; Gomperts, R.; Andres, J. L.; Raghavachari, K.; Binkley, J. S.; Gonzalez, C.; Martin, R. L.; Fox, D. J.; DeFrees, D. J.; Baker, J.; Stewart, J. J. P.; Pople, J. A. *Gaussian 92/DFT*; Gaussian: Pittsburgh, PA, 1993.
(28) Becke, A. D. *Phys. Rev. A* **1988**, *38*, 3098.
(29) Lee, C.; Yang, W.; Parr, R. G. *Phys. Rev. B* **1988**, *37*, 785.
(30) Gill, P. M. W.; Johnson, B. G.; Pople, J. A. *Int. J. Quantum Chem. Symp.* **1992**, *26*, 319. Gill, P. M. W.; Johnson, B. G.; Pople, J. A. *Chem. Phys. Lett.* **1992**, *197*, 499.
(31) Becke, A. D. *J. Chem. Phys.* **1993**, *98*, 1372.
(32) Handy, N. C.; Maslen, P. E.; Amos, R. D.; Andrews, J. S.; Murray, C. W.; Laming, G. J. *Chem. Phys. Lett.* **1992**, *197*, 506.
(33) Barone, V.; Adamo, C. *Chem. Phys. Lett.* **1994**, *224*, 432. Barone, V. *J. Chem. Phys.* **1994**, *101*, 6834.
(34) Oliphant, N.; Bartlett, R. J. *J. Chem. Phys.* **1994**, *100*, 6550.
(35) Becke, A. D. *J. Chem. Phys.* **1993**, *98*, 5648.
(36) Vosko, S. J.; Wilk, L.; Nusair, M. *Can. J. Phys.* **1980**, *58*, 1200.
(37) Hay, P. J.; Wadt, W. R. *J. Chem. Phys.* **1985**, *82*, 284.
(38) Pacios, L. F.; Christiansen, P. A. *J. Chem. Phys.* **1985**, *82*, 2664. Hurley, M. M.; Pacios, L. F.; Christiansen, P. A.; Ross, R. B.; Ermler, W. C. *J. Chem. Phys.* **1986**, 84.
(39) Stevens, W. J.; Krauss, M.; Basch, H.; Jasien, P. G. *Can. J. Chem.* **1992**, *70*, 612.
(40) Schäfer, A.; Huber, C.; Ahlrichs, R. *J. Chem. Phys.* **1994**, *100*, 5829.
(41) Huzinaga, S.; Andzelm, J.; Klobukowski, M.; Radzio-Andzelm, E.; Sakai, Y.; Tazewaki, H. *Gaussian Basis Sets for Molecular Calculations*; Elsevier: Amsterdam, 1984.
(42) Pacios, L. F.; Gomez, P. C. *Int. J. Quantum Chem.* **1994**, *49*, 817.
(43) Seijo, L.; Barandiaran, Z.; Huzinaga, S. *J. Chem. Phys.* **1991**, *94*, 3762.
(44) Li, J.; Wang, S. G.; Schwarz, W. H. E. To be submitted.
(45) Huber, K. P.; Herzberg, G. *Constants of Diatomic Molecules*; Van Nostrand Reinhold: New York, 1979.
(46) Mulliken, R. S. *J. Chem. Phys.* **1955**, *23*, 1833.
(47) Reed, A. E.; Weinstock, R. B.; Weinhold, F. *J. Chem. Phys.* **1985**, *83*, 735. Foster, J. P.; Weinhold, F. *J. Am. Chem. Soc.* **1980**, *102*, 7211. Reed, A. E.; Weinhold, F. *J. Chem. Phys.* **1985**, *83*, 1736. Reed, A. E.; Weinhold, F.; Curtiss, L. A.; Pochatko, D. J. *J. Chem. Phys.* **1986**, *84*, 5697. Reed, A. E.; Curtiss, L. A.; Weinhold, F. *Chem. Rev.* **1988**, *88*, 899.

density partitionings,[50] and Cioslowski's dynamical GAPT charges.[51] This was carried out for the EP-SCF and MP2 wave functions at the geometries optimized by the EP-MP2 method, using TZ+(d)/TZ(d) basis sets.

2.4. Crystal Embedding. In order to take account of the dominant part of the interactions in the crystal, we modeled the electrostatic effects of the atoms surrounding X_3^+ (X = Cl, Br, I) in $X_3^+AsF_6^-$ by Madelung potentials.[52,53] Mulliken net charges from ab initio calculations of individual X_3^+ and AsF_6^- using polarized triple-ζ basis sets (X_3^+, $Cl^{0.27+}Cl^{0.46+}Cl^{0.27+}$, $Br^{0.27+}Br^{0.46+}Br^{0.27+}$, $I^{0.25+}I^{0.50+}I^{0.25+}$; AsF_6^-, $As^{2.78+}$, $F^{0.63-}$) were assigned to all atoms. Their positions were chosen according to the experimental crystal structures of $X_3^+AsF_6^-$ (X = Br, I)[11,12] and to an appropriately scaled one for $Cl_3^+AsF_6^-$ (space group, $P\bar{1}$; unit cell; a = 723.4 pm, b = 534.0 pm, c = 911.7 pm, α = 95.24°, β = 84.27°, γ = 99.87°; fractional coordinates, extrapolated from those of $X_3^+AsF_6^-$ (X = Br, I)). The derived Madelung potentials were subsequently fitted in the cavity of the crystal, corresponding to the X_3^+ cluster, by about 80 point charges located at crystallographic positions of the atoms in the crystals, within 800 pm from the central halogen atom. A modified versino of Roos and Wahlgren's program[53] was used. The difference between the Madelung and fitted potentials was less than 0.0025 V.

The geometries of the X_3^+ (X = Cl, Br, I) clusters were fully optimized in the crystal fields using a nongradient procedure. The corresponding frequencies were subsequently calculated at these optimized geometries using a numerical algorithm. All calculations were accomplished on an IBM RISC/6000-350 workstation.

3. Free Cluster Cations

3.1. Geometries. Optimized bond lengths and bond angles obtained by different methods and basis sets, as well as the total energies and Mulliken net charges, are listed in Table 1 for the free cluster cations. All the molecules attain C_{2v} symmetry. No calculations of comparable accuracy were found in the literature except the recent ones by Lin and Hall[25] on I_3^+ and ICl_2^+. The effective core potential results are very similar to those obtained by the corresponding all-electron method with a comparable basis. The inclusion of d- and f-type polarization functions shortens the bond lengths considerably, as is known to be the case also for the XY dimers (for instance, without any d-function the Cl-Cl bond length is calculated about 20 pm too long). Below we will see that the geometries of Br_3^+ and I_3^+ embedded in the crystal field, when calculated with d-polarized basis sets, are still a little large but acceptably agree with the experimental ones. In the case of F_3^+, no reasonable results were found for basis sets without polarization functions.

Although the F_3^+ cluster has not yet been characterized experimentally, the optimized geometry for the free cluster, which fits smoothly into the geometries of the other clusters, and the large vibrational frequencies (see below) indicate its stability in vacuum. It may consequently be found via mass spectroscopy.

The calculated bond lengths (with d but without f functions) are well reproduced by a Schomaker−Stevenson type formula[54]

$$r = R_X + R_Y - (9.5\text{ pm})\Delta EN \qquad (1)$$

The parameters R_X, R_Y (F, 71 pm; Cl, 100 pm; Br, 115 pm; I, 135 pm) agree very well with the atomic radii in the homohalogen dimers X_2 (F, 71 pm; Cl, 99½ pm; Br, 114 pm; I, 133 pm), especially when considering that the calculational approach (see section 2.3) overestimates the bond lengths by about 1%. ΔEN is the electronegativity difference (Allred−Rochow[55]) of the central and terminal halogen atoms. The more polar the bonds in XY_2^+, the shorter they are. This tendency is even

Table 1. Geometries, Atomic Mulliken Charges, and Energies of Cluster Cations X_3^+ and XY_2^+ (X, Y = F, Cl, Br, I)

method/basis[a]	geometry $r_1 = r_2$ (pm)	geometry α (deg)	net charge[b] X_1	net charge[b] $X_2 = X_3$	total energy (au)
		F_3^+			
REP/MP2/TZ(d)	142.4	104.3	0.47	0.27	−71.6115
REP/MP2/TZ(2d)	142.9	103.2	0.48	0.26	−71.6770
REP/MP2/TZ+(2d)	142.8	103.5	0.53	0.24	−71.6815
AE/RHF/6-311(d)	137.3	109.2	(0.27)	(0.37)	−297.5142
AE/MP2/6-311(d)	143.2	104.0	0.46	0.27	−298.1436
AE/MP2/6-311+(d)	143.0	104.3	0.53	0.24	−298.1528
AE/MP2/TZV(d)	142.2	104.8	0.48	0.26	−298.1949
AE/MP2/6-311+(2df)	140.5	104.3	0.54	0.23	−298.2970
		Cl_3^+			
NEP/RHF/DZ	223.5	106.4	(0.24)	(0.38)	−43.5844
NEP/RHF/DZ(d)	199.1	106.4	(0.42)	(0.29)	−43.6552
NEP/MP2/DZ(d)	199.6	107.4	0.47	0.27	−44.0441
REP/MP2/TZ(d)	202.6	106.4	0.51	0.25	−44.1678
REP/MP2/TZ(2d)	201.4	106.8	0.48	0.26	−44.2297
REP/MP2/TZ+(2d)	201.2	106.9	0.53	0.24	−44.2318
AE/RHF/3-21	225.0	104.1	(0.23)	(0.38)	−1371.3878
AE/RHF/3-21(d)	200.7	105.9	(0.40)	(0.30)	−1371.7231
AE/MP2/3-21(d)	201.4	107.1	0.46	0.30	−1372.1257
AE/RHF/6-311(d)	200.8	106.3	(0.46)	(0.27)	−1378.0333
AE/MP2/6-311(d)	201.9	107.1	0.51	0.27	−1378.4446
AE/MP2/6-311+(d)	201.9	106.9	0.55	0.25	−1378.4563
AE/MP2/TZV(d)	203.1	106.3	0.51	0.24	−1378.4762
AE/MP2/6-311+(2df)	197.6	107.3	0.55	0.22	−1378.6296
		Br_3^+			
NEP/RHF/DZ	251.7	105.3	(0.28)	(0.36)	−38.3543
NEP/RHF/DZ(d)	231.5	104.2	(0.44)	(0.28)	−38.4264
NEP/MP2/DZ(d)	231.9	105.2	0.49	0.25	−38.7669
REP/MP2/TZ(d)	230.3	104.9	0.48	0.26	−38.3944
REP/MP2/TZ(2d)	230.9	104.0	0.36	0.32	−38.4711
REP/MP2/TZ+(2d)	230.7	104.2	0.48	0.26	−38.4739
AE/MP2/TZV(d)	230.4	105.2	0.50	0.25	−7717.5159
		I_3^+			
NEP/RHF/DZ	287.1	104.5	(0.29)	(0.36)	−33.1179
NEP/RHF/DZ(d)	268.8	103.1	(0.44)	(0.28)	−33.1807
NEP/MP2/DZ(d)	269.2	104.0	0.48	0.26	−33.4756
REP/MP2/TZ(d)	269.2	104.0	0.49	0.25	−33.6463
REP/MP2/TZ(2d)	269.6	103.6	0.39	0.31	−33.6627
		ClF_2^+			
REP/MP2/TZ+(d)	160.3	101.3	0.95	0.02	−62.5939
		BrF_2^+			
REP/MP2/TZ+(d)	171.8	99.7	1.13	−0.07	−61.0567
		IF_2^+			
REP/MP2/TZ+(d)	187.6	96.9	1.30	−0.15	−59.1776
		$BrCl_2^+$			
REP/MP2/TZ+(d)	213.3	104.3	0.64	0.18	−42.6078
		ICl_2^+			
REP/MP2/TZ+(d)	229.6	101.2	0.92	0.04	−40.7024
		IBr_2^+			
REP/MP2/TZ+(d)	246.4	102.4	0.78	0.11	−37.5301

[a] Calculated by nonrelativistic all electron (AE) or effective core potential valence-only approaches (nonrelativistic NEP or relativistic REP) at the Hartree−Fock (RHF) and correlated (MP2) levels, using different basis sets (see text). [b] MP2 Mulliken charges, SCF charge values are marked by parentheses.

(48) Boys, J. M. *Rev. Mod. Phys*. **1960**, *32*, 296. Foster, J. M.; Boys, S. F. *Rev. Mod. Phys.* **1960**, *32*, 300.
(49) Bader, R. F. W. *Atoms in Molecules*; Clarendon Press: Oxford, U.K., 1990.
(50) Schwarz, W. H. E.; Ruedenberg, K.; Mensching, L. *J. Am. Chem. Soc*. **1989**, *111*, 6926. Schwarz, W. H. E.; Lin, H. L.; Irle, S.; Niu, J. E. *J. Mol. Struct. (THEOCHEM)* **1992**, *255*, 435.
(51) Cioslowski, J. *J. Am. Chem. Soc*. **1989**, *111*, 8333.
(52) Ewald, P. P. *Ann. Phys. (Leipzig)* **1921**, *64*, 253. Bertaut, P. F. *J. Phys. Radium* **1952**, *13*, 499.
(53) Roos, B.; Wahlgren, U. *Madelung Program*; The University of Stockholm: Stockholm, 1970.
(54) Schomaker, V.; Stevenson, D. P. *J. Am. Chem. Soc*. **1941**, *63*, 37.
(55) Allred, A. L.; Rochow, E. G. *J. Inorg. Nucl. Chem*. **1958**, *5*, 264.

more pronounced than for the hetero-halogen diatomics XY,[45] where the "ionic contraction" turns out to be proportional to (−6.5 pm)ΔEN only. It also indicates an increased effective electronegativity of the central atom in XY_2^+.

Concerning the reasonability of eq 1, we note that Pauling defined the electronegativity differences with the help of thermodynamic bond energy stabilizations caused by covalent−ionic resonance and that bond energy increases tend to go along with bond length contractions. The assumption, that bonds between second row atoms N, O, and F are expanded because of lone pair repulsions [56−58] is not sufficient to explain the bond length trends of the various trihalogen species at the level of 1 pm accuracy. The recently proposed covalent radius of fluorine (54 pm) corresponds, according to eq 1, to binding of F to atoms of medium electronegativity (∼2.2). Claiming that the repulsive effect between the lone pairs varies in the same manner as the electronegativity difference also implies that corrections to constant effective radii are necessary. Another example of nonconstant radii has recently been given with reference to lanthanide contractions.[59]

The central X^+ atom is isoelectronic with a divalent chalcogen atom. Accordingly the bond angles are similar to those of the corresponding chalcogen halides (for instance, $\alpha(OF_2) = 103.3°$, $\alpha(SCl_2) = 100°$ or 103°, $\alpha(SeBr_2) = 98°$ [60−62]). The angles of XY_2^+ are a few degrees larger because the halogen cation is smaller than the chalcogen atom. Pure pσ-bonds correspond to 90° bond angles. The real bond angles are somewhat larger, in order to accommodate the sum of van der Waals radii of the two terminal atoms (see Figure 2). The nearer the terminal ligands to the central atom, and the heavier and more space demanding they are, the larger the bond angle is. The expansion of the bond angle results in slightly bent bonds[63] (vide infra). An alternative explanation is as follows. The lighter the central atom, the greater the tendency for s−p hybridization and the lesser the tendency for p−d hybridization, the larger the bond angle is. The following formula reproduces the angles of the trihalogen cations very well:

$$\alpha = 96.8° + \delta_c + 2\delta_t \qquad (2)$$

The increment values of the central atoms are $\delta_c(F) = 7.6°$, $\delta_c(Cl) = 4.8°$, $\delta_c(Br) = 2.9°$, and $\delta_c(I) = 0°$ (reference value) and for the terminal atoms $\delta_t(F) = 0°$ (reference value), $\delta_t(Cl) = 2.3°$, $\delta_t(Br) = 2.8°$, and $\delta_t(I) = 3.6°$. Again, the arguments of lone pair repulsion (i.e., using van der Waals radii) or of electronegativity differences result in the same trend predictions. According to the VSEPR-model[64] the bond angle should also be smaller, the larger the electronegativity of the ligand is. The Walsh rules[65] are also in accordance with the strongly bent C_{2v} geometry for the 20-valence electron systems X_3^+ and XY_2^+, while a linear $D_{\infty h}$ geometry occurs for the well-known 22-valence electron anions X_3^- and XY_2^-; see Figure 3. We note

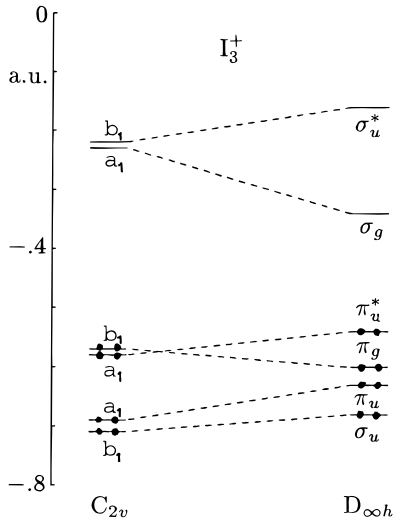

Figure 3. Molecular orbital levels (spin−orbit averaged) of I_3^+, emerging from the in-plane I 5pσ-AOs (the vertical pπ-MOs are omitted), for the C_{2v} ground state and the $D_{\infty h}$ saddle point state.

the large gap between occupied and unoccupied MOs for C_{2v} symmetry, indicating that MP2 perturbation theory should yield reasonable results for the bent ground state.

The $D_{\infty h}$ geometries of the cationic clusters correspond to the transition state for inversion. The large inversion barriers (72, 72, 68, and 59 kcal/mol calculated at the EP/MP2/TZ+(d) level for species F_3^+, Cl_3^+, Br_3^+, and I_3^+, respectively) demonstrate the stability of the bent geometries against distortion. In addition to the symmetric ground state potential energy minimum, there exists a second minimum on the same potential energy surface. It corresponds to a loosely bound complex of X_2 and X^+ of linear $C_{\infty v}$ symmetry $[X-X\cdots X]^+$, with $r_1 \ll r_2$. This complex has indeed four real frequencies, e.g., for species $\{I_2\cdots I\}^+$ (with bond parameters $r_1 = 263$ pm, $r_2 = 327$ pm) 53.7, 72.2, 92.1, and 246.9 cm^{-1} at the RHF/TZ+(d) level. However, upon reducing r_2 a little, or upon approaching the X^+ vertically to X_2, the ground state geometry is easily reached. So, this metastable geometry of X_3^+ is not expected to be found in the free state.

3.2. Charge Distributions. Effective atomic charges in molecules depend both on the method (or definition) used to determine them[66] and on the quality of charge density distribution (e.g., the applied basis set). The most striking feature in Table 1 is the drastic increase of positive charge on the central atom upon inclusion of polarization functions. Figure 4 exhibits the density change (∼+0.2) upon adding an f-function to the 6-311+(2d) basis. Also, without electron correlation the central charge is too low, in the case of F_3^+ by ∼0.2. This holds for the Mulliken charges shown in Table 1, as well as for the other charges not shown there.

Static Mulliken charges, natural charges, and Cioslowki's dynamical charges from MP2 calculations using TZ+(d) basis sets for all the free clusters are listed in Table 2. For comparison Mulliken and natural charges for the X_3^+ clusters (X = Cl, Br, I) in the Madelung potentials are also given. Concerning the *homonuclear* species, all the different charge definitions yield the same qualitative picture: $X^{1/4+}X^{1/2+}X^{1/4+}$. The larger charge on the central atom is in agreement with experimental NQR results[7,67] and also with valence bond concepts.

The Mulliken charges on the central atom of the free *hetero*atomic clusters are larger than those of the terminal atoms by about 0.5 ΔEN. (The natural charges are even larger by

(56) Gillespie, R. J.; Robinson, E. A. *Inorg. Chem.* **1992**, *31*, 1960.
(57) Wells, A. F. *Structural Inorganic Chemistry*, 5th ed.; Clarendon Press: Oxford, U.K., 1984; pp 287 ff.
(58) Sanderson, R. T. *Polar Covalence*; Academic Press: New York, 1983.
(59) Wang, S. G.; Schwarz, W. H. E. *J. Phys. Chem.* **1995**, *99*, 11687.
(60) Pierce, L.; Jackson, R.; DiCianni, N. *J. Chem. Phys.* **1961**, *35*, 2240.
(61) Stammreich, H.; Forneris, R.; Sone, K. *J. Chem. Phys.* **1955**, *23*, 972.
(62) Milne, J. *Polyhedron* **1985**, *4*, 65.
(63) Wiberg, K. B.; Murcko, M. A. *J. Mol. Struct. (THEOCHEM)* **1988**, *169*, 355.
(64) Gillespie, R. J. *Molekülgeometrie*; Verlage Chemie: Weinheim, Germany, 1975; *Chem. Soc. Rev.* **1992**, *21*, 59. Gillespie, R. J.; Hargittai, I. *The VSEPR Model of Molecular Geometry*; Prentice Hall: Englewood Cliffs, NJ, 1991.
(65) Walsh, A. D. *J. Chem. Soc.* **1953**, 2260. Bent, H. A. *Chem. Rev.* **1961**, *61*, 275. Buenker, R. J.; Peyerimhoff, S. *Chem. Rev.* **1974**, *74*, 127.
(66) Meister, J.; Schwarz, W. H. E. *J. Phys. Chem.* **1994**, *98*, 8245.

Table 2. Atomic Charges on the Central and Terminal Atoms from MP2 Calculations in Free Clusters X_3^+ and XY_2^+ (X, Y = F, Cl, Br, I) and in the X_3^+ Clusters Embedded in Madelung Potentials of X_3AsF_6[a]

	central					terminal				
cluster	Mul	nat	Cio	de-fi	Bad	Mul	nat	Cio	de-fi	Bad
F_3^+	0.54	0.52	0.59	0.41	0.48	0.23	0.24	0.21	0.30	0.26
Cl_3^+	0.55	0.57	0.52	0.41	0.39	0.23	0.22	0.24	0.30	0.30
Br_3^+	0.49	0.52	0.57			0.25	0.24	0.22		
I_3^+	0.51	0.52	0.57			0.24	0.21	0.21		
ClF_2^+	0.95	1.42	1.31			0.02	−0.21	−0.15		
BrF_2^+	1.13	1.73	1.43			−0.07	−0.36	−0.22		
IF_2^+	1.30	1.96	1.57			−0.15	−0.48	−0.28		
$BrCl_2^+$	0.64	0.82	0.85			0.18	0.09	0.08		
ICl_2^+	0.92	1.17	1.11			0.04	−0.06	−0.09		
IBr_2^+	0.78	0.90	0.89			0.11	0.05	0.05		
$Cl_3^+AsF_6^-$	0.66	0.56				0.20	0.25			
						0.14	0.19			
$Br_3^+AsF_6^-$	0.64	0.55				0.21	0.25			
						0.15	0.20			
$I_3^+AsF_6^-$	0.61	0.56				0.22	0.24			
						0.17	0.20			

[a] Mul = Mulliken charge; nat = Weinhold et al. natural bond orbital charge; Cio = Cioslowski GAPT charge; de-fi = charge based on atomic density fitting;[50] Bad = topological Bader charge.

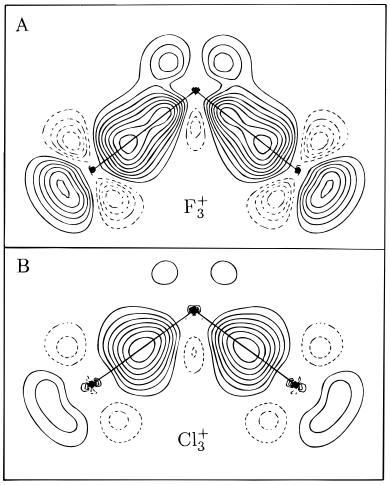

Figure 4. RHF-density change of F_3^+ (A) and Cl_3^+ (B) upon adding one f-polarization function to the 6-311+(2d) basis. Values of contour lines: 0.01*n* e/Å^3, $n = \pm1,\pm2,...$ Density increase, —; density decrease, - -.

about 1 ΔEN.) This trend is also in agreement with the NQR results. As usual, the natural charges are larger than the Mulliken ones and the Cioslowski charges are in between (compare with ref 66). So, the formal description as $X^+(Y^0)_2$ seems very reasonable, especially for the heteroatomic cluster ions.

We have also analyzed the charge distribution of F_3^+ and Cl_3^+ with the help of the "oriented independent atoms in molecules" approach.[50] The directions and occupations of the atomic ground state orbitals of the open p-valence shells of the halogen atoms are adjusted to simulate the electron density of the cluster ions. The results are presented in Table 3. The terminal atoms have, in addition to the occupied s^2, two nearly occupied p-AOs, corresponding to three lone pairs, while the central atom has only one (nearly) occupied p-AO (the pπ) in addition to s^2, corresponding to two lone pairs. The bonding pσ-AO on the terminal halogens is less occupied than the one on the central atom, corresponding to bond pairs being polarized toward the central atom.

The total p-shell occupation on the terminal atoms is larger than on the central atom, as indicated by the density-fitted charges (de-fi) in Table 2. The shape of the charge distribution of the independent atoms in the molecule is determined by the direction and occupation (p_i) of their p-AOs and can be described by the quadrupolar and asymmetry parameters

$$q = p_1 - \overline{p_{2,3}} \quad a = |p_2 - p_3| \tag{3}$$

where p_2 and p_3 are the two most similar occupation values. The terminal halogens with two lone pairs in two p-AOs (nearly) vertical to the X_c-X_t bonds are disklike with (nearly) axial symmetry around the bond direction; q is negative, and a is small. The central halogen, forming two bonds in the molecular plane, is cigar-shaped with a p-lone pair vertical to the plane; it has a positive q-parameter and is slightly asymmetric ($a \approx 0.2$). Finally we note that the terminal pσ-AOs are weakly rotated inside (see Figure 5 and Table 3).

When the independent oriented atoms are allowed to interact, bond formation is accompanied by electron density deformation. This so-called chemical deformation density

$$\delta\varrho = \varrho(\text{molecule}) - \sum\varrho(\text{oriented independent atoms}) \tag{4}$$

is shown in Figure 6. The two lone pairs on the central atom correspond to the two maxima of $\delta\varrho$ in the symmetry plane

Table 3. Occupations of Atomic Ground State Orbitals of the Open Valence *p*-Shell of the Halogen Atoms in F_3^+ and Cl_3^+ [a]

		X_c		X_t	
cluster	AO				
F_3^+	pπ	2.00	(2.00)	1.99	(2.00)
	p*n*	1.39	(1.51)	1.95	(2.00)
	pσ	1.21	(1.22)	0.76	(0.63)
	ω (deg)			1.2	(0.4)
	q	0.70	(0.64)	−1.21	(−1.37)
	a	0.19	(0.29)	0.03	(0.00)
Cl_3^+	pπ	1.93	(1.94)	1.89	(1.93)
	p*n*	1.41	(1.45)	1.81	(1.87)
	pσ	1.25	(1.24)	1.01	(0.89)
	ω (deg)			2.2	(2.2)
	q	0.60	(0.60)	−0.84	(−1.00)
	a	0.16	(0.21)	0.08	(0.06)

[a] pπ = occupation of the vertical p-AOs, p*n* = of the *p*-AOs pointing in the direction of a lone pair, pσ = of the third orthogonal p-AO related to the bond pairs. Angle ω, see Figure 5; q = atomic quadrupolar parameter; a = asymmetry of the atomic quadrupole. X_c and X_t denote the central and terminal halogen atoms. AE/MP2/6-311+(2df) calculations. RHF-values in are parentheses.

(67) Merryman, D. J.; Corbett, J. D.; Edwards, P. A. *Inorg. Chem.* **1975**, *14*, 428.

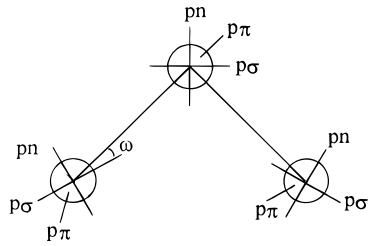

Figure 5. Direction of independent atoms' valence p-AOs in X_3^+.

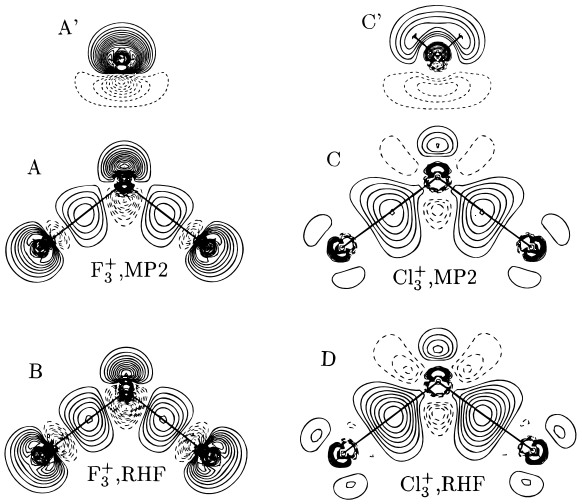

Figure 6. Chemical deformation density $\delta\rho$ of F_3^+ (A, A′, B) and Cl_3^+ (C, C′, D), $\delta\rho = \rho$(molecule) $- \sum\rho$(oriented independent atoms): (A, A′, C, C′) AE/MP2/6-311+(2df) calculations; (B, D) the corresponding RHF-densities; (A, B, C, D) in the molecular plane, where the lines connect the nuclei; (A′, C′) in the symmetry plane vertical to the molecular plane, where the lines connect the central nucleus with two $\delta\rho$-maxima corresponding to the lone pairs. Values of contour lines: $0.1n$ e/Å^3 with $n = \pm1, \pm2,$ ... for F_3^+, and $0.05n$ e/Å^3 for Cl_3^+. Density increase, —; density decrease, - -.

perpendicular to the molecular plane (see Figure 6A′,C′). The lone pair charge polarizations in the molecular plane are much more pronounced for F than for Cl. The maxima of the bond charge accumulations lie exactly on the straight interatomic connections. However, $\delta\rho$ is not axially symmetric but slightly more extended into the molecular triangle, corresponding to weakly inward bent bonds. We note again the density changes due to electron correlation, which reduces both the bond and lone pair features.

3.3. Bonding. The bonding in the trihalogen cluster cationic compounds was interpreted in the literature at a qualitative level: (a) by an ionic model involving two intracluster pσ bonds, (b) by a covalent bridging model with d^2sp^3 hybridization, and (c) by an ionic model with sp^3 hybridization. Shamir[7] favored a hybrid of b and c. It was considered that no exclusive model was appropriate.

The NBO analysis (Table 4), as well as the density analysis of section 3.2, confirm that there are two polar−covalent bonds of dominant pσ-type. Corresponding to 20% larger electronegativity of positively charged halogens X^+, the bonds are polarized toward the central atom of X_3^+, but toward the terminal atoms of XY_2^+ if Y's electronegativity is ~0.5 Pauling units larger than that of X. This is also nicely documented by plots of the bonding molecular orbitals, using the localized representation (Figure 7). The bond orders (as defined by Mayer[68]) of F_3^+ andf Cl_3^+ are presented in Table 5. They are about unity and very similar to the ones in the corresponding

(68) Mayer, I. *Chem. Phys. Lett.* **1983**, *97*, 270.

Table 4. Composition of the Natural Hybrid AOs ($s^a p^1 d^b$) Derived from SCF Densities and Their Contribution (%) to the Two Bonding σ NBOs

cluster	X_c	a	b	%	β^a	δ^b	Y_t	a	b	%
F_3^+	F_c	0.10	0.002	68	94.5	4.9	F_t	0.02	0.003	32
Cl_3^+	Cl_c	0.11	0.014	62	93.8	6.3	Cl_t	0.04	0.016	38
Br_3^+	Br_c	0.08	0.014	62	93.7	5.6	Br_t	0.03	0.015	38
I_3^+	I_c	0.07	0.014	62	92.2	5.9	I_t	0.03	0.013	38
ClF_2^+	Cl_c	0.09	0.022	38	91.9	4.7	F_t	0.08	0.002	62
BrF_2^+	Br_c	0.06	0.016	30	89.9	4.9	F_t	0.09	0.002	70
IF_2^+	I_c	0.06	0.013	24	91.9	2.5	F_t	0.09	0.002	76
$BrCl_2^+$	Br_c	0.08	0.015	53	96.5	3.9	Cl_t	0.06	0.018	47
IC_2^+	I_c	0.07	0.019	44	95.8	2.7	Cl_t	0.06	0.011	56
IBr_2^+	I_c	0.07	0.016	51	91.6	5.4	Br_t	0.04	0.011	49

[a] β = angle between the two hybrids of the central atom. [b] δ = difference between hybrid and bond directions ($\beta + 2\delta$ = bond angle α).

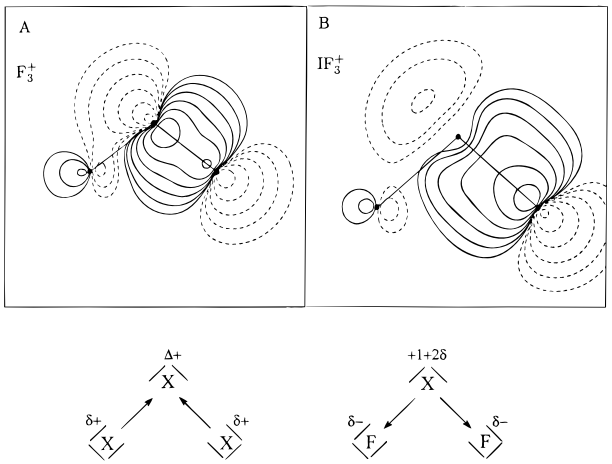

Figure 7. Localized MOs corresponding to the p−p−σ-bond (A) in F_3^+ and (B) in IF_2^+ and the respective VB-diagrams of X_3^+ and XF_2^+ species. Values of contour lines: $0.1(2^n)$ e/Å^3 with $n = 0, 1, 2,$ ....

Table 5. Mayer Bond Orders

molecule	SCF	MP2	molecule	SCF	MP2
F_2	1.072	0.907	Cl_2	1.103	1.048
F_3^+ (F_c-F_t)	0.968	0.933	Cl_3^+ (Cl_c-Cl_t)	1.138	1.118
(F_t-F_t)	0.099	0.113	(Cl_t-Cl_t)	0.128	0.152

diatomics. The X_c-X_t bonds in X_3^+ have a slightly elliptic charge distribution (ϵ = 0.04 in F_3^+ and 0.035 in Cl_3^+), indicating weak π-character. There is also some bonding interaction between the two terminal atoms, especially at the correlated MP2 level (see Table 5).

The bond critical points in F_3^+ and Cl_3^+ (Figure 8) are shifted toward the terminal atoms by 7 and 5%, respectively, corresponding to the higher electronegativity of the central halogen. The three valence shell charge concentrations of the central atom are typical for a divalent chalcogen, while the two charge concentrations of the terminal atoms closely resemble the ones in the dihalogen molecules. The trend in the Laplacian plots from F_3^+ to Cl_3^+ continues to I_3^+, given in Figure 4a of ref 25.

The natural bond hybrids are p-AOs with little s-admixture and even less d-admixture, far less than to expect significant sp^3 or d^2sp^3 hybridization in the solid. The admixtures are smaller for the terminal than for the central atoms and also smaller for heavier than for lighter atoms. The angles between the bond hybrids (90−96°) are smaller than the bond angles, by about 10°. Also, Bader's bond paths[49] are very slightly bent inward, by about 2°, which is hardly visible in Figure 8. Both features are in accord with $\delta\rho$ (see end of section 3.2). This small bending due to nonbonded interactions is of typical magnitude for normal single bonds.[63]

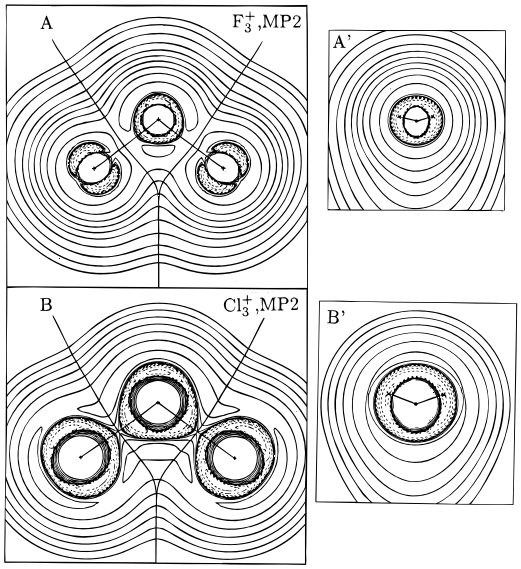

Figure 8. Laplacian of the 6-311+(2d)/MP2 density. (A, A′) F_3^+; (B, B′) Cl_3^+; (A, B) in the molecular plane; (A′, B′) in the symmetry plane perpendicular to the molecular plane. Contour line values: $0.01(2^n)$ au ($n = 0, 1, 2, ...$). Atomic core features are dropped. The additional lines in A, B represent the bond paths and the atomic boundaries as defined by Bader; the additional straight lines in A′, B′ connect the central nucleus with its two lone pair charge concentrations.

The present discussion refers to species X_3^+ and XY_2^+, where the terminal atom Y is the more electronegative one. In the "inverted" trihalogen cations YX_2^+, the central atom Y, because of its higher electronegativity, resists becoming positively charged, resulting in different electronic and geometric structures of YX_2^+. Preliminary calculations of symmetric FI_2^+ yield several local minima on the potential energy surface. The lowest one of C_{2v} symmetry corresponds to a central F^- bonded at an obtuse angle to two I^+ ($\alpha = 132°$ (MP2) or 139° (MP3)). The bonds are much longer than in IF_2^+, namely, $r_{1,2} = 208$ pm, which is approximately equal to $R_X + R_Y$ without any polar bond shortening, as observed for the stable clusters ions XY_2^+ (see eq 1). Another configuration of symmetric FI_2^+ (only about $3^1/_2$ kcal/mol higher in energy) occurs for an F^- vertically above I_2^{2+} with a comparatively short bond between the two I atoms ($r = 265$ pm). The F−I distances are even longer than before ($r_{1,2} = 238$ pm), corresponding to an acute bond angle of $\alpha = 67°$ and a purely ionic, noncovalent interaction between F^- and I_2^{2+}. Thus, the symmetric species YX_2^+ are not expected to be stable in the solid state. We note the experimental evidence for the asymmetric geometries of FCl_2^+, $ClIBr^+$, ClI_2^+, and BrI_2^+, with the more electronegative atom being in the terminal position.[7]

3.4. Vibrational Frequencies. The free cluster cations with C_{2v} symmetry possess four independent harmonic valence force constants (f_r, f_{rr}, $f_{r\alpha}$, f_α), which determine the vibrational modes of A_1^b (bending), A_1^{st} (symmetric stretch), and B_1 (asymmetric stretch) symmetry. The calculated values of force constants and vibrational frequencies are presented in Table 6. Without d-functions, the results are seriously too small. Addition of a second d-set changes the force constants nonnegligibly. As usual, the Hartree−Fock results for the diagonal force constants (f_r, f_α) and vibrational frequencies seem too large. All force constants show a general tendency: the more electronegative the central and terminal atoms are, the more they increase. All force constants are significantly positive, so all species are predicted to be stable in the free state (vacuum).

The bond stretch force constants f_r and frequencies A_1^{st}, I_1^{st} are a few percent smaller than those of the X_2 molecules,[45] while those of XY_2^+ are a little larger than those of XY. This harmonizes with the reduced bond lengths of XY_2^+.

4. Cluster Cations in the Crystal

4.1. Geometries. The calculations have been performed for Cl_3^+, Br_3^+, and I_3^+ in the crystal field of the AsF_6^- compounds, using the extended TZ+(d) basis sets. The results are compared with experimental X-ray data in Table 7. As usual, correlation (MP2) expands the bond lengths, here by 1−2 pm. The hybrid DFT approach yields even longer bond lengths, and the bond angles are also increased. As to be expected from previous experience with heavy atomic systems,[69,70] the pure DFT method (BLYP) yields bond lengths and angles that are too large.

Due to the asymmetric surrounding in the crystal, the C_{2v} symmetry of the cluster cations is weakly broken. The bond lengths differ by 1 pm experimentally, but by 4−5 pm in our model calculation. The probably most reliable MP2 calculations yield bond lengths which are 6 pm too large, indicating errors due to the neglect of *f* and higher angular momentum basis functions and of nonelectrostatic interactions. The calculated MP2 bond angles are very reliable. Comparison with the free ions shows that the crystal field expands the bond lengths by ~3 pm and reduces the bond angles by ~2.5°.

4.2. Charge Distributions. Upon embedding X_3^+ (X = Cl, Br, I) in the Madelung potentials of $X_3^+AsF_6^-$, the central atom becomes more positive by about $+0.1|e|$. Because of the adjacent F^- atoms of AsF_6^-, the Madelung potential is repulsive for an electron at the site of the cationic atoms and this potential is larger at the central atom with two adjacent F^- than at the terminal atoms with only one adjacent F^-; see Figure 2 (e.g., for I_3^+, $V_c = 6.1$ V, $V_t = 5.3 \pm 0.2$ V). Accordingly, the electron density at the central atom is further decreased by the Madelung potential. This agrees well with the NQR experimental result for $I_3^+AlCl_4^-$.[7,67]

4.3. Stability. The stability of the cluster cations in solid compounds depends on several factors. For instance, a larger exothermicity of the reaction

$$XY_2^+ + X^- \xrightarrow{\Delta E} X_2 + Y_2 \qquad (5)$$

where X^- may be supplied by the counterions, will reduce the stability of the compounds under discussion. We have estimated ΔE to be of the order of 6−7 eV for I_3^+, IBr_2^+, ICl_2^+, IF_2^+, Br_3^+, $BrCl_2^+$, BrF_2^+, Cl_3^+, and ClF_2^+, but nearly 10 eV for F_3^+. This indicates the probable instability of F_3^+ in the solid state.

4.4. Force Constants and Frequencies. By comparison of the different experiments and our calculations of vibrational frequencies (Table 6), the following conclusions can be drawn. The MP2 calculations give the best results, the pure DFT (BLYP) calculations are the worst ones, and the hybrid approach (B3LYP) is intermediate. Both DFT approaches yield splittings of the symmetric and antisymmetric stretch which are drastically too large. The SCF frequencies are too large, as usual. The MP2 values are only slightly larger with an average error of $+15 \pm 20$ cm^{-1}. The crystal field has only a small influence on the stretch vibrations, changing them by a few percent at most. However, the bending mode, which is comparatively low in the free clusters, is increased by the field by as much as 50%.

In Table 8, we compare the experimentally determined structural and vibrational parameters with calculated estimates,

(69) Wang, S. G. Doctoral Thesis; University of Siegen; Shaker Verlag, Aachen, 1994.
(70) Liao, M. S. Doctoral Thesis; University of Siegen; Shaker Verlag, Aachen, 1993.

Table 6. Vibrational Frequencies (cm^{-1}) and Force Constants (N/cm) of XY_2^+ and of XY in Vacuum

	freq of XY_2^+			force const of XY_2^+				f_r of XY	
method/basis	A_1[b]	A_1^{st}	B_1^{st}	f_r	f_{rr}	$f_{r\alpha}$	f_α	calc	exp[a]
				F_3^+					
REP/MP2/TZ(d)	417	843	945	4.63	0.182	0.283	0.569	5.18	4.70
REP/MP2/TZ(2d)	410	869	975	4.92	0.143	0.288	0.557		
AE/RHF/6-311(d)	420	932	957	5.00	0.595	0.088	0.575		
AE/MP2/6-311(d)	411	788	890	4.11	0.149	0.289	0.553		
AE/MP2/6-311+(d)	408	797	904	4.21	0.134	0.277	0.546		
AE/MP2/TZV(d)	416	872	983	4.95	0.163	0.263	0.565		
AE/MP2/6-311+(2df)	430	900	993	5.18	0.270	0.289	0.604		
				Cl_3^+					
NEP/RHF/DZ	135	412	439	1.89	0.152	0.034	0.109		
NEP/RHF/DZ(d)	212	492	524	2.69	0.211	0.078	0.268		
NEP/MP2/DZ(d)	199	472	485	2.42	0.309	0.081	0.235		
REP/MP2/TZ(d)	194	503	523	2.78	0.304	0.083	0.224	3.22	3.23
REP/MP2/TZ(2d)	193	489	507	2.62	0.306	0.085	0.221		
AE/RHF/3-21	135	417	443	1.92	0.118	0.032	0.110		
AE/RHF/3-21(d)	208	471	497	2.46	0.219	0.091	0.260		
AE/MP2/3-21(d)	194	449	457	2.19	0.310	0.090	0.222		
AE/RHF/6-31	145	414	445	1.93	0.139	0.042	0.126		
AE/RHF/6-31(d)	212	508	546	2.90	0.215	0.084	0.267		
AE/RHF/6-311(d)	211	517	556	3.00	0.203	0.081	0.267		
AE/MP2/6-311(d)	199	480	502	2.54	0.281	0.087	0.235		
AE/MP2/6-311+(d)	199	484	508	2.60	0.276	0.091	0.234		
AE/MP2/TZV(d)	193	505	529	2.82	0.287	0.084	0.221		
				Br_3^+					
NEP/RHF/DZ	77	244	261	1.50	0.097	0.025	0.081		
NEP/RHF/DZ(d)	107	301	323	2.29	0.130	0.053	0.158		
NEP/MP2/DZ(d)	101	295	310	2.17	0.195	0.056	0.136		
REP/MP2/TZ(d)	101	290	302	2.08	0.208	0.057	0.137	2.43	2.46
REP/MP2/TZ(2d)	100	280	289	1.93	0.194	0.060	0.137		
				I_3^+					
NEP/RHF/DZ	51	164	175	1.09	0.066	0.018	0.057		
NEP/RHF/DZ(d)	66	205	219	1.70	0.088	0.034	0.097		
NEP/MP2/DZ(d)	61	201	212	1.62	0.126	0.035	0.083		
REP/MP2/TZ(d)	62	203	214	1.65	0.126	0.035	0.084	1.82	1.72
REP/MP2/TZ(2d)	60	198	208	1.56	0.126	0.038	0.080		
				ClF_2^+					
REP/MP2/TZ+(d)	334	813	818	4.85	0.313	0.090	0.432	4.08	4.48
				BrF_2^+					
REP/MP2/TZ+(d)	264	723	715	4.67	0.206	0.033	0.318	3.72	4.06
				IF_2^+					
REP/MP2/TZ+(d)	215	656	652	4.16	0.084	0.006	0.226	3.25	3.62
				$BrCl_2^+$					
REP/MP2/TZ+(d)	161	436	431	2.72	0.253	0.062	0.188	2.85	2.82
				ICl_2^+					
REP/MP2/TZ+(d)	134	405	400	2.63	0.152	0.033	0.145	2.43	2.38
				IBr_2^+					
REP/MP2/TZ+(d)	85	265	271	2.08	0.139	0.036	0.112	2.06	2.07

[a] Experimental values from the data given by ref 45.

obtained by appropriate scaling of the theoretical results for the free cluster ions. For the cases of missing experimental results, the theoretical estimates are predictions with an accuracy of ±2 pm for r, ±4° for α, ±30 cm^{-1} for the ν, and ±10 cm^{-1} for the $A_1^{st} - B_1^{st}$ splitting. Here, we have assumed that different surroundings of the trihalogen cations modify the geometric and spectral parameters by less than the given uncertainties. Some of the assignments of the experimental IR and Raman spectra are obviously incorrect (compare, e.g., the discussion in refs 11 and 13) and are put in parentheses in Table 8. In general, $\nu(B_1) > \nu(A_1^{st})$. We note that the opposite is calculated for $(Br,I)(F,Cl)_2^+$. Several, though not all, experimentalists support this finding in the investigated cases of BrF_2^+ and ICl_2^+.[16,71,72]

The X_3^+ units possess six independent harmonic valence force field constants in the crystal. Since the C_{2v} symmetry is only weakly broken, it is reasonable to assume $f_r = f_{r'}$ and $f_{r\alpha} = f_{r'\alpha}$, as the experimentalists did. While B_1 determines $f_r - f_{rr'}$, the remaining three constants $f_r + f_{rr'}$, $f_{r\alpha}$, and f_α are still not completely fixed by the other two experimental frequencies of A_1 character. For variable choice of $f_{r\alpha}$, the resulting f_r and f_α vary on elliptical curves.[73]

Sawodny and Rai[74] suggested for cases $m_X > m_Y$ to choose $f_{r\alpha}$ so that f_α(exp) takes its minimal value. This somewhat arbitrary recipe corresponds to

(71) Surles, T.; Quarterman, L. A.; Hyman, H. H. *J. Fluorine Chem.* **1973**, *3*, 293.
(72) Forneris, R.; Tavares-Forneris, Y. *J. Mol. Struct.* **1974**, *23*, 241.
(73) Siebert, H. *Anwendungen der Schwingungspektroskopie in der Anorganischen Chemie*; Springer: Berlin, 1966. Fadini, A. *Molekülkraftkonstanten*; Steinkopff: Darmstadt, Germany, 1976. Herzberg, G. *Infrared and Raman Spectra of Polyatomic Molecules*; Van Nostrand Reinhold: New York, 1945.
(74) Sawodny, W.; Rai, S. N. *J. Mol. Struct.* **1969**, *30*, 56.

Table 7. Geometries, Vibrational Frequencies, and Internal Force Constants of Cluster Cations X_3^+ (X = Cl, Br, I) Calculated in the Madelung Fields

	geometry			freq (cm^{-1})			force const (N/cm)			
method	r_1 (pm)	r_2 (pm)	α (deg)	A_1^b	A_1^{st}	B_1^{st}	f_r	f_{rr}	$f_{r\alpha}$	f_α
				Cl_3^+						
MP2/6-311+(d)	202.7	204.2	103.7	270	502	510	2.66	0.399	0.152	0.448
B3LYP/6-311+(d)	205.5	208.1	105.5	258	401	475	2.02	0.637	0.093	0.406
RHF/TZ+(d)	201.8	202.3	103.0	291	559	584	3.27	0.274	0.158	0.507
MP2/TZ+(d)	203.3	205.0	103.2	274	511	522	2.79	0.426	0.166	0.447
BLYP/TZ+(d)	208.3	212.1	106.5	250	356	451	1.75	0.631	0.057	0.371
B3LYP/TZ+(d)	205.3	207.7	105.2	266	421	489	2.17	0.619	0.104	0.417
exp[11] [a]	198	198	103	225	489	508	2.61	0.184	0.060	0.314
exp[1]				225	490	508	2.48			0.356
				Br_3^+						
RHF/TZ+(d)	229.8	232.0	102.5	159	330	343	2.66	0.225	0.122	0.382
MP2/TZ+(d)	230.9	234.3	102.6	149	305	316	2.36	0.324	0.130	0.339
BLYP/TZ+(d)	234.9	242.2	107.4	139	227	277	1.67	0.443	0.047	0.289
B3LYP/TZ+(d)	232.1	237.1	105.5	147	263	298	1.98	0.460	0.086	0.319
exp[11]	226.6	227.5	102.5	124	293	297	2.06	0.192	0.052	0.216
exp[19,11]				227, 238	280−295	288				
				I_3^+						
RHF/TZ+(d)	269.5	273.6	101.6	100	216	228	1.90	0.127	0.068	0.266
MP2/TZ+(d)	270.6	275.6	101.4	95	202	215	1.73	0.184	0.078	0.239
BLYP/TZ+(d)	273.6	285.6	107.2	91	144	189	1.25	0.273	0.030	0.222
B3LYP/TZ+(d)	270.9	278.9	105.1	95	172	202	1.48	0.282	0.051	0.233
exp[11,12]	266.0	266.9	101.8	110	205	211	1.61	0.097	0.065	0.273
exp[3]				114	207	233	1.92	0.156	0.070	0.294

[a] In the case of Cl_3^+, the bond lengths listed in the exp row are the estimated values[11] used to calculate the corresponding force constants from the experimental frequencies.

Table 8. Geometries and Frequencies of Trihalogen Cluster Cations[a]

species	$r_1 \approx r_2$ (pm)	α (deg)	A_1^b (cm^{-1})	A_1^{st} (cm^{-1})	Δ^{st} [b] (cm^{-1})
F_3^+	140	102	500	850	+100
Cl_3^+	197	104	230; MP, 270	500; MP, 511	+12; MP, +11
	198	103	225	490	+18
Br_3^+	227	102	120; MP, 149	295; MP, 305	+11; MP, +11
	227	102	124	280−295	+4
			(∼230)		(−2)
I_3^+	267	101	75; MP, 95	205; MP, 202	+12; MP, +13
	267	101	110, 114	205, 207	+6, +26
ClF_2^+	157	99	400	790	+5
	158	103	373−396	785−811	+8 to +27
	154	96	(520−558)	(518−529)	(+40, −24)
BrF_2^+	169	97	320	700	−8
	171	94	291−308	688−713	−10 to −15
	169	91	344−370	(625)	(∼−30, ∼0, +10)
IF_2^+	185	94	260	635	−4
$BrCl_2^+$	210	102	190	425	−4
ICl_2^+	227	99	160	395	−5
	231	97	143−161	359−400	0, −7, −16
	227	92			(+6, +20)
IBr_2^+	244	100	100	255	+6
			124, 127	236−256	0, +10

[a] First entry: scaled calculated values of the free species (EP/MP2/TZ(d); $r_{1,2}$ − 3 pm; α − 2½°; 1.2$\nu(A_1^b)$; 0.97$\nu(A_1^{st})$ MP: calculated value in the Madelung potential). Second entries (where given): ranges of experimental literature values (see ref 7 and Table 7); values in parentheses are probably incorrectly assigned. [b] Δ^{st} = splitting $\nu(B_1^{st}) - \nu(A_1^{st})$.

$$f_{r\alpha}/f_\alpha = \sin\alpha/(1 + Q + \cos\alpha) = S \quad (6)$$

where $Q = m_X/m_Y$. Thakur and Rai[75] suggested for the opposite case ($m_X < m_Y$) to choose a smaller value of $f_{r\alpha}$, which approximately corresponds to

$$f_{r\alpha}/f_\alpha \approx \sin^2\alpha/(1 + Q + \cos\alpha)[(1 + Q)^2 + 1 - 2\cos^2\alpha]^{1/2} = T \quad (7)$$

This latter recipe was used by Christe et al.[11] for the X_3^+ species. It is now appropriate to compare the ratios S and T with our calculated ones in Table 9. Thakur and Rai's choice for $f_{r\alpha}$ is definitely too low. Also the variation of $f_{r\alpha}/f_\alpha$ among the XY_2^+ species is not well reproduced by the empirical rules. Since the $f_r - f_{r\alpha}$ curves are rather steep, a small reduction of $f_{r\alpha}$ results in a large reduction of f_r. While there is reasonable agreement between the calculated (MP2) and experimental frequencies, as mentioned above, this is not the case for the calculated and *experimentally adjusted force constants*. The theoretical force constants (see Tables 6 and 7) vary smoothly upon changing the central and terminal halogens from F to Cl to Br to I, whereas the experimental choice[11] results in unexpected orders I > Cl > Br for $f_{r\alpha}$ and Br > Cl > I for f_{rr} and f_α (see Table 7).

(75) Thakur, S. N.; Rai, S. N. *J. Mol. Struct.* **1970**, *5*, 320.

Table 9. Calculated Ratio of Force Constants $f_{r\alpha}/f_{\alpha}$, and Sawodny's and Thakur's Assumptions, *S* and *T*, respectively

cation	theoretical $f_{r\alpha}/f_{\alpha}$[a]	*S*	*T*
F_3^+	0.50	0.55	0.22
Cl_3^+	0.38 (0.37)	0.55	0.22
Br_3^+	0.43 (0.38)	0.55	0.22
I_3^+	0.45 (0.33)	0.55	0.22
IBr_2^+	0.32	0.41	0.14
$BrCl_2^+$	0.33	0.32	0.09
ClF_2^+	0.21	0.37	0.11
ICl_2^+	0.23	0.22	0.05
BrF_2^+	0.10	0.19	0.04
IF_2^+	0.03	0.13	0.02

[a] For the free ion. In parentheses: cation in Madelung potential.

5. Summary

Pseudopotential MP2 calculations with extended basis sets yield satisfactory results for the X_3^+ and XY_2^+ (with X heavier than Y) halogen cluster cations. Polarization functions are important for geometries, charge distributions, force constants, etc., which, however, is not unexpected (compare for instance ref 76); all halogen atoms and their ions are quite polarizable species. The requirement of d-functions, even for the fluorine species, should not be taken as evidence of d-orbital participation in s−p−d hybridization, which would demand a much higher d-population than in the 1% range obtained here.

RHF/DF hybrids, and especially the pure density functional approaches, work less satisfactorily. For instance, the Becke correction results in bond lengths that are definitely too large.

All compounds have rigid ground states. They possess two σ-bonds of p−p type. The bond angles are somewhat larger than 90°, especially for a lighter central halogen and a heavier terminal one. The bond angles are about 10° larger than the angles between the hybrids of the central atom (∼95°), except for IF_2^+ and ICl_2^+, which have a "large enough" central atom. The widening of the bond angle can at least partially be explained by nonbonded repulsions between the terminal atoms. Their internuclear separations are of the order of the sums of their van der Waals radii (F, 1.3 Å; Cl, 1.6 Å; Br, 1.8 Å; I, 2.1 Å). This results in slightly bent bond paths. There also exist weak covalent and dispersion forces between the terminal atoms.

F_3^+ is special. While correlation increases both the bond lengths and bond angles in all the other trihalogen cations, the bond angle reduction does not occur in F_3^+. The terminal fluorine atoms in F_3^+ are already so strongly overlapping with each other that the bond length expansion of ∼6 pm due to electron correlation is accompanied by a significant bond angle decrease of ∼5°.

In the valence bond approach these compounds may be interpreted as mixed-valence ones with monovalent neutral terminal atoms and divalent central atoms with a positive formal charge, as represented in Figure 7. The bond polarity and electron density distribution in the cluster ions is governed, as usual, by the electronegativity differences, with the formally X^+ divalent pseudochalcogen central atom being about 20% more electronegative than X^0 (i.e., the Allred−Rochow electronegativity of F^+ is 5.0 and of I^+ is 2.7). Accordingly, the central atom in X_3^+ carries a larger positive charge than the terminal ones. This holds even for F_3^+, which is a stable compound with a positively charged $F_c^{0.5+}$ atom, provided reaction 5 is made impossible. XY_2^+ cluster cations, where the X is the lighter, more electronegative atom, correspond to complexes of the type $X^- \cdots Y_2^{2+}$, which have different structures than those considered here.

Analysis of the bond lengths and force constants leads to the conclusion that the two bonds in X_3^+ are very similar to the bonds in X_2, while the bonds in XY_2^+ are slightly shorter and stronger than in XY, indicating the increased ionic stabilization.

The crystal field of the surrounding does not seriously influence the geometry and the stretching modes but increases the bending force constants and bending frequencies significantly. Without explicitly accounting for orbital interactions and dispersion interactions with the counterions, the bond lengths were obtained a few picometers too long, and the $f_{rr'}$ coupling force constants (i.e., the A_1-B_1 splitting of the bond stretch frequencies), too large. Otherwise there is reasonable agreement with reliable experimental spectroscopic results.

However, Sawodny's and Thakur's rules[74,75] for determining the experimentally unknown force constants $f_{r\alpha}$ do not work well in the present case. Therefore the experimentally derived force constants need some revision. Predicted geometries and vibrational frequencies were displayed in Table 8.

Acknowledgment. We acknowledge the assistance of Dr. H. Möller, Dr. S. G. Wang, and Ing. D. H. Duong. We are grateful to the Deutsche Forschungsgemeinschaft and the Fonds der Chemischen Industrie for financial support.

IC950305S

(76) Cioslowski, J.; Surján, P. R. *J. Mol. Struct. (THEOCHEM)* **1992**, *255*, 9.